

# Configuration Requirements for 21-cm Forest Background Quasar Searches with the Moon-based Interferometer

Siyuan Zhang,<sup>1</sup> Qi Niu,<sup>1</sup> Yichao Li,<sup>1,\*</sup> and Xin Zhang<sup>1,2,3,†</sup>

<sup>1</sup>Key Laboratory of Cosmology and Astrophysics (Liaoning) & College of Sciences, Northeastern University, Shenyang 110819, China

<sup>2</sup>National Frontiers Science Center for Industrial Intelligence and Systems Optimization, Northeastern University, Shenyang 110819, China

<sup>3</sup>Key Laboratory of Data Analytics and Optimization for Smart Industry (Ministry of Education), Northeastern University, Shenyang 110819, China

The 21-cm forest offers a powerful cosmological probe of the thermal history and small-scale structure of the intergalactic medium during the Epoch of Reionization (EoR). Its success, however, critically depends on the availability of high-redshift radio-loud quasars (HzRLQs) as background sources. In this work, we investigate the configuration requirements for a Moon-based low-frequency radio interferometer aimed at maximizing the detection of HzRLQs for future 21-cm forest studies. Building upon a previously developed quasar luminosity function (QLF), we forecast HzRLQ abundances under various array configurations. Assuming a total survey area of  $10^4 \text{ deg}^2$  and 1 year of observation, we compare continuum surveys with 10 MHz bandwidth and 21-cm forest surveys with 5 kHz resolution. Our results show that a minimum collecting area of  $\sim 6500 \text{ m}^2$  enables detection at  $z \sim 6$ , while SKA-like arrays ( $N_{\text{st}} = 512$ ) extend the detection limit to  $z \sim 10$  for 21-cm forest survey and  $z \sim 16$  for continuum survey. Larger arrays with  $N_{\text{st}} = 2048$  can reach  $z \sim 11$  in 21-cm forest mode. We also explore configurations that maintain fixed collecting areas while increasing the number to enhance survey efficiency. This boosts source detection but significantly increases the data volume and computational demands. These results underscore the importance of optimizing array design for different survey goals and balancing sensitivity, spectral resolution, and data management. A well-designed Moon-based array could open a new observational window on reionization and early cosmic structure formation.

Keywords: Quasars — Radio loud quasars — Reionization — HI line emission — Surveys

## I. INTRODUCTION

The 21-cm signal from the hyperfine transition of neutral hydrogen (HI) has become a powerful cosmological probe for the study of the early Universe, in particular, the Dark Ages, the Cosmic Dawn, and the Epoch of Reionization (EoR) [1]. Recently, Shao et al. [2] proposed a novel cosmological probe known as the 21-cm forest, which provides a unique probe of small-scale structures during the EoR. The 21-cm forest relies on the absorption characteristics of HI in the intervening structures along the line of sight with respect to the spectra of the bright background radio sources, such as radio-loud quasars. This technique provides valuable insights into the nature of dark matter (DM) and its role in shaping small-scale structure formation [3–5].

Breakthroughs in the 21-cm forest have been difficult to achieve because of ongoing challenges in both analytical modeling and observations. Because of the absence of analytical models, the parameter inference of the 21-cm forest relies on complex small-scale simulations. The substantial computational cost of simulations poses a significant challenge to constrain the astrophysical parameters. Recently, several new approaches have been proposed to address this challenge, including the deep-learning-driven likelihood-free parameter inference methods [6] and a halo-model-based analytical model for the one-dimensional power spectrum of the 21-cm forest [7].

Moreover, the detection of the 21-cm forest power spectrum remains challenging due to the limited sensitivity of current low-frequency observational facilities. This constraint is especially critical for the identification of high-redshift radio-loud quasars (HzRLQs), which serve as essential background sources. While optical and near-infrared surveys have extended quasar observations to redshifts beyond 6 [8, 9], the number of detected radio-loud quasars at such high redshifts remains small. A recent study [10] examined the abundance of HzRLQs and confirmed that the observations are still constrained by flux limitations even with the next-generation low-frequency radio telescope arrays, such as the low-frequency Square Kilometre Array (SKA-Low). This scarcity presents a significant obstacle to advancing 21-cm forest studies.

Advances in space technology now make it possible to utilize the far side of the Moon - a radio-quiet environment that is uniquely shielded from Earth's ionospheric aberrations and man-made radio frequency interference (RFI)[11–13]. This pristine electromagnetic environment provides an extraordinary platform for groundbreaking low-frequency radio astronomy observations [14]. The RFI-free conditions on the far side of the Moon allow the detection of weak cosmological signals, in particular, the 21-cm HI line from the Dark Ages, Cosmic Dawn, and EoR. [15, 16].

In this work, we thoroughly explore the survey strategies for HzRLQs with the future moon-based low-frequency array. Although the technology for building a large radio interferometric array like SKA-Low on the far side of the Moon remains underdeveloped, this paper explores its immense potential and the fundamental configuration requirements for detecting HzRLQs. Specifically, we analyze two deployment scenarios: one involving variations in the effective receiving area and the other involving changes in the station diameter. These approaches

\*Corresponding author, liyichao@mail.neu.edu.cn

†Corresponding author, zhangxin@mail.neu.edu.cn

are designed to address existing observational limitations. Additionally, we provide a detailed comparison of the HzRLQs under both the continuum survey and the 21-cm forest survey. However, these strategies also introduce new engineering challenges related to array optimization and data processing. Such a Moon-based observatory will provide transformative insights into the formation of the cosmic structure at the dawn of the universe and during its first billion years [17–19].

The paper is organized as follows: In Section II, we describe the construction of the luminosity function for predicting the abundance of HzRLQs and the improvement of the model by including the obscuration effects. In Section III, we present various scenarios for the construction of the low-frequency radio array on the Moon. In Section IV, we present our results, including the influence of obscuration effects on the prediction of high-redshift quasars and how to build future moon-based arrays with the most significant detection of quasars and cost savings. Finally, in Section V, we summarize our conclusions and outline future research directions.

## II. LUMINOSITY FUNCTION MODEL

### A. Physical-Driven Model

This study extends the physical-driven model established in previous work by incorporating the impact of optical observation biases on the detection of obscured quasars. A brief summary of the model is provided here, with detailed descriptions available in [10]. The key steps in constructing the model are described as follows:

1. **Calculate the black hole (BH) mass function.** Quasars are driven by the active behavior of BHs at the centers of galaxies. Therefore, the first step is to determine the abundance of BHs in galaxy centers. We use a dark matter halo mass function in Sheth–Tormen form [20] to describe the abundance of halos of different masses at different redshifts. We assume that each halo hosts a galaxy and that each galaxy contains a central BH. The BH mass function is then derived from the halo mass function using the mass relationship between BHs ( $M_{\text{BH}}$ ) and their corresponding halos ( $M_{\text{h}}$ ) [10, 21],

$$M_{\text{BH}}(M_{\text{h}}, z) = A \left( \frac{M_{\text{h}}}{10^{12} M_{\odot}} \right)^{\frac{5}{3}} \left( \frac{\xi(z)(1+z)^3}{\Omega_{\text{m}}} \right)^{\frac{5}{6}} M_{\odot}, \quad (1)$$

where  $A$  is the amplitude parameter and  $\xi(z)$  is the dimensionless parameter related to redshift  $z$ . In this work, we adopt the best-fit value  $A \simeq 3.2 \times 10^6$  from [10].

2. **Determine the quasar duty cycle with quasar luminosity function (QLF).** The quasar duty cycle  $D_{\text{q}} = t_{\text{q}}/t_{\text{H}(z)}$  quantifies the fraction of black holes in the quasar phase, where  $t_{\text{q}}$  is the quasar lifetime and  $t_{\text{H}(z)}$  is the cosmic age at redshift  $z$ . Assuming Eddington-limited accretion, we constrain  $t_{\text{q}}$  by fitting observational data of the QLF at high redshifts [22, 23].

3. **Determine the fraction of radio-loud quasars.** We assume that 10% of quasars are radio-loud [according to observational experience, e.g. 24–26]. The fraction of radio-loud quasars over a flux threshold  $F_{\text{th}}$  is determined by integrating the radio-loudness distribution function  $N(R)$ ,

$$\epsilon(M_{\text{h}}, F_{\text{th}}) = \int_{R_0}^{\infty} dR N(R), \quad (2)$$

where the lower-bound  $R_0 = R_0(M_{\text{BH}}(M_{\text{h}}, z), F_{\text{th}})$  is a function of black hole mass and flux threshold.

4. **Estimate the abundance of HzRLQs.** The abundance of HzRLQs is then estimated by integrating the weighted halo mass function,

$$N(\Delta z, \Delta \Omega, F_{\text{th}}) = \int_{\Delta z, \Delta \Omega} dV \int dM_{\text{h}} 10\% D_{\text{q}} \epsilon(M_{\text{h}}, F_{\text{th}}) \Phi_{\text{h}}(M_{\text{h}}), \quad (3)$$

where  $\Delta z$  and  $\Delta \Omega$  are the redshift bin and survey sky area,  $dV$  is the cosmological volume element, and  $\Phi_{\text{h}}(M_{\text{h}}) = dn/dM_{\text{h}}$  represents the halo mass function.

### B. Obscuration-corrected QLF

The obscuration in the optical band may significantly affect predictions of the abundance of the HzRLQs. The distribution and nature of dust play a critical role in the observational properties of active galactic nuclei (AGNs). In particular, the molecular clouds and high-extinction regions can obscure AGNs, rendering them undetectable in optical surveys [27]. Quasars, especially at high redshifts, can be heavily obscured by dust in the optical band, which complicates their identification. This obscuration effect has been extensively studied, with findings indicating that a considerable fraction of AGNs are missed in optical surveys due to dust extinction [28]. Since the construction of the HzRLQ abundance model depends on the QLF in the optical band, dust obscuration in the optical band may lead to an underestimation of the abundance of HzRLQs. This underestimation has direct implications for studies such as the 21-cm forest, which rely on a complete census of background radio sources.

The obscuration renders the quasar luminosity in certain wavelength bands. To ensure the accuracy of the observed high-redshift quasar population, their luminosity function can be corrected by introducing an obscuration fraction, which is estimated based on the observations in the X-ray band [29].

$$f_{\text{obs}} = \min[\psi_{\text{max}}, \max[\psi_0 - \beta \log(L_{\text{X}}/L_{\text{X},0}), \psi_{\text{min}}]], \quad (4)$$

where  $\phi_0 = 0.73$ ,  $\psi_{\text{max}} = 0.84$ ,  $\psi_{\text{min}} = 0.2$ ,  $\beta = 0.24$ ,  $L_{\text{X},0} = 10^{43.75} \text{ erg s}^{-1}$  [30, 31]. The X-band luminosity is estimated via the bolometric correction factor of the hard X-ray band [32]:

$$K_{\text{X}}(L_{\text{bol}}) = \frac{L_{\text{bol}}}{L_{\text{X}}} = a \left( 1 + \left( \frac{\log(L_{\text{bol}}/L_{\odot})}{b} \right)^c \right) \quad (5)$$

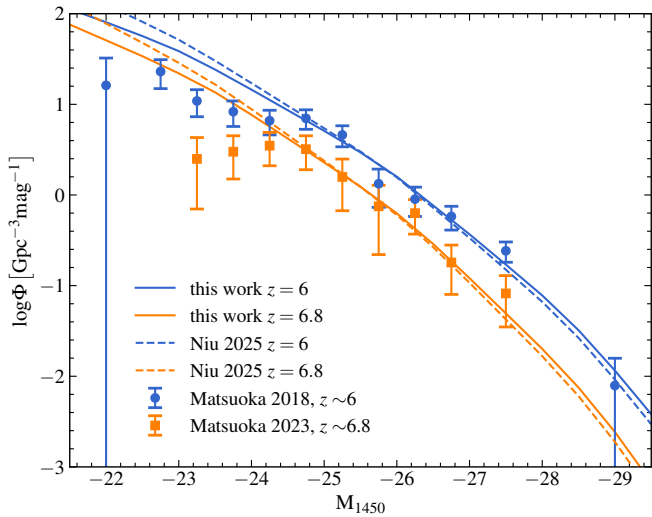


FIG. 1: Comparison of the best-fit QLF with and without considering the optical-band obscuration effect. Blue and orange curves denote models at redshifts  $z = 6$  and  $z = 6.8$ , respectively. Solid lines illustrate models with obscuration effects in our work, whereas the dotted lines represent models without considering the obscuration effect. The blue and orange errorbars show the measurements at  $z \sim 6$  from Matsuoka et al. [22] and  $z \sim 6.8$  from Matsuoka et al. [23]. Owing to observational incompleteness, the first two data points on the faint end are omitted.

where  $a = 10.96$ ,  $b = 11.93$ , and  $c = 17.79$ . It is worth noting that the obscuration fraction function is primarily constrained using X-ray selected AGN samples at redshifts  $z \lesssim 5$ . Due to the limited observational data available for quasars at higher redshifts, the redshift evolution of the obscuration fraction remains uncertain. In this work, we therefore adopt a simplified approach and assume a redshift-independent obscuration fraction, acknowledging that this may introduce some uncertainties in our predictions.

We correct the luminosity function by multiplying the luminosity function of total quasars with the fraction of unobscured to obtain the luminosity function of the optically observed quasars,

$$\Phi = \Phi_{\text{total}}(M_{1450}, z) \times (1 - f_{\text{obsc}}). \quad (6)$$

We compare the best-fit model with and without considering the obscuration effect in Figure 1. The QLF model with considering the obscuration effect, is shown with the solid curve. The dashed curve represents the best-fit model from Niu et al. [10]. The QLF model is fitted to the data by adjusting the mean quasar lifetime  $t_q$  until the likelihood function is maximized. Two main datasets are used in this work, i.e., one set of data is at  $z \sim 6$  [22], and the other one is at  $z \sim 6.8$  [23]. For the fits at  $z = 6$  and  $z = 6.8$ , the least-square values are about 7.79 and 3.78, respectively. Taking into account the obscuration effect, the luminosity function has  $t_q = 10^{5.79}$  at  $z = 6$ ,  $t_q = 10^{5.76}$  at  $z = 6.8$ .

By comparing the results with and without obscuration effects, we find that incorporating obscuration leads to a slightly flatter QLF, a trend observed at both redshifts considered in

our analysis. This is mainly because low-luminosity quasars are more likely to be obscured by dust, making them less likely to be detected in optical surveys. Including the obscuration effect can thus partially alleviate the discrepancy between theoretical models and observational QLF data at the faint end. However, the improvement is limited. As mentioned above, the obscuration fraction is based on low-redshift data, and its possible redshift evolution is not considered in this work. Additionally, the incompleteness of the observed sample at the faint end may still be the dominant factor contributing to the observed deviation.

### III. MOON-BASED INTERFEROMETER CONFIGURATION

Literature research indicates that a significant detection of HzRLQs requires a radio interferometer with a sensitivity comparable to that of SKA-Low [10]. SKA-Low is designed to probe the early Universe through radio observations. It consists of 131 072 log-periodic dipole antennas, grouped into 512 stations, each containing 256 antennas [39]. Approximately 50% of these stations are concentrated within a 1 km diameter central core, while the rest are distributed along three spiral arms extending up to 74 km. The total effective collecting area is about 419 000 m<sup>2</sup>, providing exceptional sensitivity to faint radio signals. Operating within a frequency range of 50 MHz to 350 MHz, SKA-Low can observe the 21-cm signal at redshifts approximately between  $z \sim 3$  and  $z \sim 27$ , covering key cosmic epochs such as the EoR and the Cosmic Dawn.

The observational noise variance of the radio interferometer is estimated via,

$$\sigma = \sqrt{2} \frac{k_B T_{\text{sys}}}{A_{\text{eff}}} \frac{1}{\sqrt{N_{\text{st}}(N_{\text{st}} - 1)\Delta t \Delta \nu}}, \quad (7)$$

where  $k_B$  is the Boltzmann constant,  $A_{\text{eff}}$  refers to the effective receiving area of a station,  $N_{\text{st}}$  is the number of stations,  $\Delta \nu$  is the frequency channel width, and  $\Delta t$  is the integration time.  $T_{\text{sys}}$  is the system temperature, and it is consist of,

$$T_{\text{sys}} = T_{\text{sky}} + T_{\text{rx}}, \quad (8)$$

where  $T_{\text{sky}}$  is the mean brightness temperature from the sky and takes the form of

$$T_{\text{sky}} = \left( 2.73 + 25.2 \times (408/\nu_{\text{MHz}}(z))^{2.75} \right) \text{ K}, \quad (9)$$

where  $\nu(z)$  represents the frequency in MHz corresponding to redshift  $z$ .

In this work, we consider the surveys are carried out with a continuum survey, which has the flux measurements integrated over the frequency band of 10 MHz to enhance the signal-to-noise ratio for continuum source detection. Due to the limited frequency resolution, the following 21-cm forest analysis requires additional deep-field observations. We also consider a 21-cm forest survey with spectrum resolution of 5 kHz. Such high-frequency resolution significantly reduces the detection

ability for HzRLQs, but it is fine enough for the 21-cm forest analysis without additional follow-up observations.

We assume  $T_{\text{rx}} = 0.1T_{\text{sky}} + 40\text{K}$  [33] and also assume a constant total survey area  $S_{\text{tot}} = 10000 \text{ deg}^2$  and total observation time  $t_{\text{tot}} = 1 \text{ yr}$ . The observational noise variance may vary according to different effective collecting areas and survey efficiency.

*a. Varying the effective collecting area* We consider the future construction of low-frequency interferometric arrays of varying sizes on the far side of the Moon. Using SKA-Low as a reference, we maintain a constant station diameter of  $D = 40 \text{ m}$ . The array size ranges from  $N_{\text{st}} = 8, 32, 128,$  and  $512$  up to  $2048$  stations. Notably, an array with  $512$  stations is comparable in size to the current SKA-Low, while the  $2048$ -station configuration represents a more ambitious scenario, with an effective collecting area exceeding one square kilometer.

*b. Varying the station diameter* The solid angle of the field of view (FoV) for a single pointing is estimated using the primary beam size of the station given by  $\Omega \sim (1.2\lambda/D_{\text{st}})^2$ , where  $D_{\text{st}}$  is the diameter of a station. For the subsequent analysis, we use the wavelength  $\lambda$  corresponding to  $150 \text{ MHz}$  to estimate the FoV. By varying the station diameter, the FoV for a single pointing changes, thereby affecting the survey efficiency, while keeping the total survey area and observation time constant. To maintain consistency with the current SKA-Low, we ensure the total effective collecting area remains at  $\sim 419000 \text{ m}^2$ , and varying the number of stations and the diameter of the station simultaneously. In particular, we consider the following station configurations:  $\{(N_{\text{st}}, D_{\text{st}})\} = \{(512, 40 \text{ m}), (2048, 20 \text{ m}), (8129, 10 \text{ m})\}$ .

#### IV. RESULTS AND DISCUSSIONS

Using the configuration parameters introduced in Section III, we estimate the system noise variance level for each case. We use 10 times of the noise variance level as the lower bound of the integration of the predicted luminosity function to forecast the abundance of HzRLQs.

##### A. Configuration requirements with continuum survey

The number of HzRLQs detected (with their flux over 10 times the corresponding noise level) in continuum surveys is shown in Figure 2, where different colors represent results for various interferometer size configurations. Since the predicted abundance depends on the width of the redshift bins, we fix the redshift bin  $\Delta z = 0.5$  for the analysis of continuum surveys. Generally, the number of detected HzRLQs significantly reduced as redshift increased. The gray histogram corresponds to an array of eight  $40 \text{ m}$ -diameter stations, with an effective collecting area of  $6546.875 \text{ m}^2$ . This configuration enables the detection of approximately  $10^3$  radio-loud quasars at  $z \sim 5$  and provides statistically significant detections ( $N > 10$ ) up to  $z \sim 10$ .

Increasing the number of stations dramatically enhances detection capabilities. With  $N_{\text{st}} = 128$ , the number of detected HzRLQs increases by an order of magnitude at each redshift bin, and the redshift detection limit extends to  $z \sim 16$ .

As discussed in Section III, an interferometer with  $512$   $40 \text{ m}$ -diameter stations achieves an effective collecting area comparable to that of the current SKA-Low. An even more ambitious configuration, with  $N_{\text{st}} = 2048$ , would push the total collecting area beyond one square kilometer. Such an interferometer would enable the robust detection of HzRLQs up to the beginning of the EoR or even Cosmic Dawn.

Increasing the effective collecting area of an interferometric array can significantly enhance its sensitivity to HzRLQs. Beyond simply scaling up the array, we also explore an alternative strategy that maintains the same total collecting area – comparable to that of the SKA – while boosting survey efficiency by employing smaller station diameters to achieve a larger field of view. The corresponding results are shown in Figure 3, where different colors indicate configurations with varying station numbers and sizes.

Our findings demonstrate that even without increasing the total collecting area, the detection capability for HzRLQs can be improved by increasing the number of stations and reducing the diameter of each station. This configuration effectively enhances sky coverage and survey speed. However, it is important to note that such a design imposes substantial demands on the system, particularly in terms of data transmission, communication bandwidth, and computational resources required for data processing. These factors pose significant challenges for the data analysis pipelines of interferometric arrays and must be carefully considered in future instrument design.

Our analysis shows that the detectability of HzRLQs in continuum surveys is strongly dependent on both the size and configuration of the interferometric array. Increasing the number of stations significantly boosts sensitivity, enabling detections out to higher redshifts, with large arrays ( $N_{\text{st}} \gtrsim 512$ ) capable of probing the EoR and potentially even Cosmic Dawn. Moreover, we demonstrate that optimizing array layout – by increasing station number while reducing individual station size – can further enhance survey efficiency without increasing the total collecting area. This approach increases the survey field of view and improves detection rates but introduces substantial challenges in data transmission and processing. These trade-offs highlight the need for carefully balanced array designs that optimize both scientific return and technical feasibility in future low-frequency radio surveys targeting HzRLQs.

##### B. Configuration requirements with 21-cm forest survey

Through wide-area continuum surveys, large low-frequency radio interferometric arrays have the potential to detect a substantial number of high-redshift radio-loud quasars (HzRLQs). By integrating over frequency channels, continuum observations significantly enhance the signal-to-noise ratio. However, this integration comes at the expense of frequency resolution, which is critical for 21-cm forest power spectrum analysis. As a result, continuum detections often require dedicated follow-

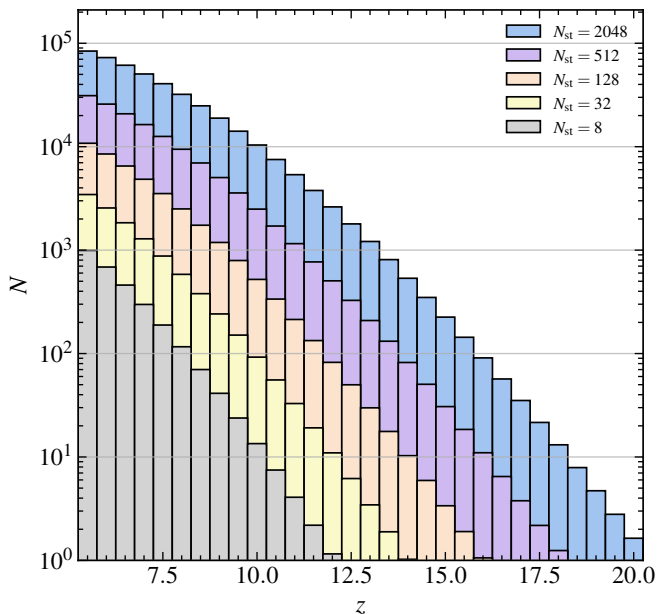


FIG. 2: The number of HzRLQs detected with continuum survey as a function of redshift with different sizes of interferometer. The results with  $N_{\text{st}} = 8, 32, 128,$  and  $512$  up to  $2048$  stations are shown in different colors.

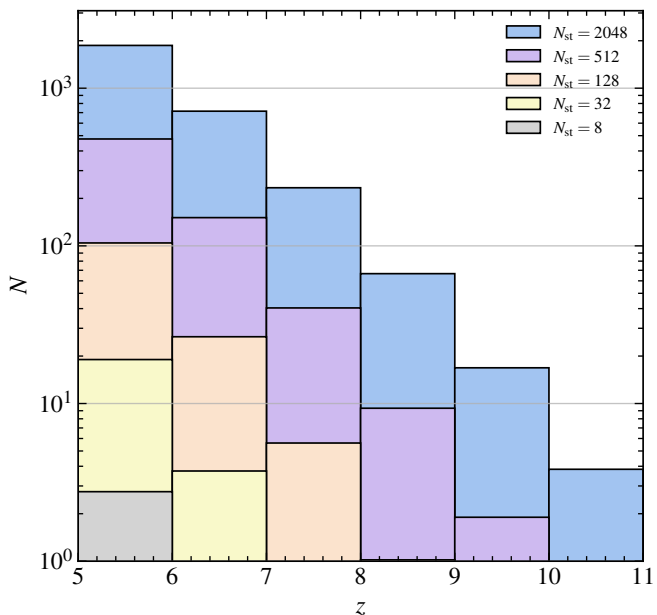


FIG. 4: Similar to Figure 2, but for 21-cm forest survey with 5 kHz frequency resolution.

up observations to probe fine spectral structures. In this work, we assume a frequency resolution of 5 kHz for 21-cm forest surveys, and investigate how different array sizes impact the detectability of HzRLQs. The corresponding results are shown in Figure 2, where different colors represent low-frequency arrays of various sizes. For this analysis, we adopt a redshift bin

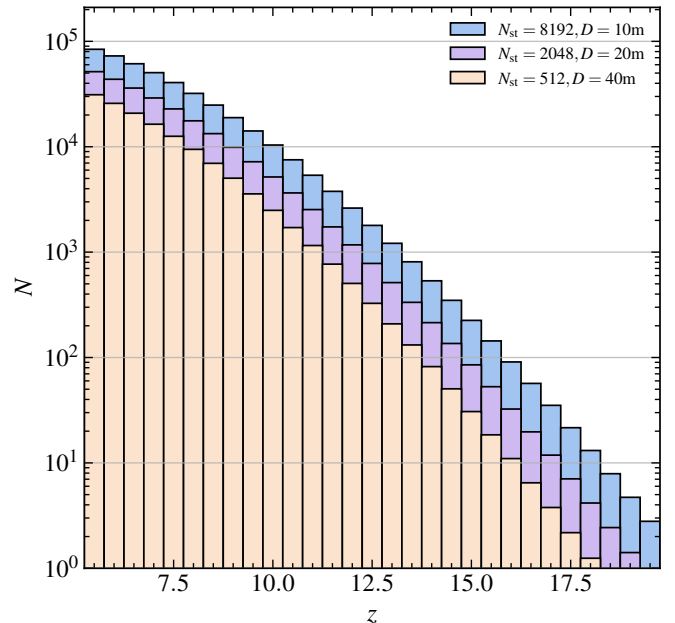


FIG. 3: The number of HzRLQs detected with continuum survey as a function of redshift with different diameters of station and number of station configurations. The results with  $\{(N_{\text{st}}, D_{\text{st}}) = (512, 40 \text{ m}), (2048, 20 \text{ m}), (8129, 10 \text{ m})\}$  are shown in different colors.

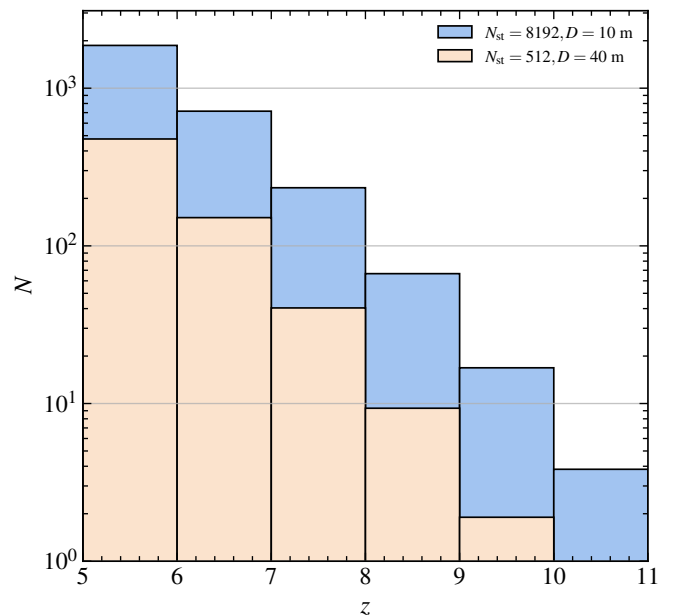


FIG. 5: Similar to Figure 3, but for 21-cm forest survey with 5 kHz frequency resolution.

width of  $\Delta z = 1$ .

Compared to continuum observations, the high spectral resolution required for 21-cm forest studies leads to a significant increase in observational noise, thereby reducing the detectability of HzRLQs. For a mini-size array with only  $n = 8$  stations, detecting HzRLQs beyond  $z > 5$  becomes

nearly impossible. However, for an array comparable to the ground-based SKA, with  $n = 512$  stations, a moderate number of HzRLQs can still be detected, even though sensitivity remains lower than in continuum mode. In this configuration, the detection limit extends to approximately  $z \sim 10$ , which is sufficient for meaningful cosmological studies using the 21-cm forest. For extremely large arrays with  $n = 2048$  stations, the detection redshift limit can be further extended to  $z \sim 11$ .

We also explore a scenario in which the total effective collecting area is constant, but the number of stations is increased while reducing the diameter of each station. This approach enhances the field of view and survey efficiency, potentially improving the HzRLQ detection rate. The results are presented in Figure 5, where different colors indicate different configurations of station number and size. Our findings show that reducing the station diameter by a factor of four and simultaneously increasing the number of stations by a factor of sixteen can substantially increase both the number of detectable HzRLQs and the maximum redshift reached. However, this gain in survey efficiency comes with a trade-off: significantly greater data transmission, storage, and processing demands, posing major challenges for interferometric data analysis.

The detectability of HzRLQs in 21-cm forest surveys is governed by a complex interplay between array configuration and spectral resolution. While continuum surveys benefit from lower noise levels due to frequency integration, 21-cm forest observations require high spectral resolution and thus face higher noise. Larger and denser interferometric arrays can extend detection capabilities to higher redshifts, but they also introduce considerable computational and infrastructural challenges. Achieving an optimal balance between sensitivity, resolution, and data processing efficiency will be essential for the successful design and operation of future low-frequency radio arrays targeting the 21-cm forest.

### C. Challenges in construction

As we discussed in the previous sections, the substantial increase in the number of base stations brings a series of complex challenges in hardware design, data processing, and data storage [34].

The construction of large-scale radio arrays faces significant technical challenges as the number of antenna elements increases. Each station comprises multiple critical components, including antennas, low-noise amplifiers, filters, and analog-to-digital converters. With the dramatic rise in real-time data throughput, network congestion becomes a serious concern, particularly in distributed or remote configurations [35].

These challenges are further amplified for space-based applications such as lunar interferometer arrays, where observational data must be downlinked to ground-based data centers for further analysis. The resulting data volumes present substantial hurdles for storage, transport, and long-term data management.

From a computational perspective, system scaling results in the combinatorial growth of processing complexity. The

calibration and imaging pipelines generate intermediate data products that often exceed the volume of raw observational data by orders of magnitude [36, 37].

Furthermore, dense station layouts heighten the risk of self-generated radio frequency interference (RFI), which can significantly degrade data quality. Mitigating these effects requires meticulous array design, including optimized station geometries, careful component isolation, and advanced electromagnetic shielding techniques [38].

Overall, these technical and infrastructural challenges must be carefully considered in the design of next-generation radio arrays, particularly those targeting high-resolution, wide-field observations such as the 21-cm forest.

## V. CONCLUSION

This work investigates the scientific prospects and technical design requirements for detecting high-redshift radio-loud quasars (HzRLQs) using a Moon-based low-frequency interferometric array, with the goal of enabling 21-cm forest studies during the Epoch of Reionization (EoR) and Cosmic Dawn.

We begin by improving the quasar luminosity function (QLF) model through the inclusion of dust obscuration effects. Since optical surveys tend to miss heavily obscured sources, particularly at the faint end, we introduce an X-ray-based correction to account for this bias. The obscuration-corrected QLF yields more accurate predictions for the abundance of HzRLQs and helps partially mitigate discrepancies between theoretical models and observations.

Assuming a total survey area of  $10^4 \text{ deg}^2$  and an integration time of 1 year, we analyze the detectability of HzRLQs in two complementary observing modes: continuum surveys and 21-cm forest surveys. For continuum surveys, we adopt a bandwidth of 10 MHz, enabling significant signal-to-noise enhancement through frequency integration. In contrast, 21-cm forest observations require fine frequency resolution – assumed to be 5 kHz in this work – to resolve small-scale absorption features, which increases thermal noise and reduces source detectability.

We evaluate detection performance across a range of array sizes. For the smallest configuration considered ( $N_{\text{st}} = 8$  stations with 40 m diameter), continuum surveys can detect HzRLQs up to  $z \sim 10$ , but the 21-cm forest survey becomes ineffective beyond  $z \sim 5$ . For SKA-scale arrays ( $N_{\text{st}} = 512$ ), continuum surveys can detect quasars out to  $z \sim 16$ , while 21-cm forest observations remain feasible up to  $z \sim 10$ . For an extremely large array with  $N_{\text{st}} = 2048$ , the detection limit of the 21-cm forest survey extends to  $z \sim 11$ , supporting deeper exploration of the EoR.

We further explore configurations that maintain a fixed total collecting area ( $\sim 419\,000 \text{ m}^2$ ) but increase the number of stations by reducing the station diameter. This strategy improves field-of-view and survey efficiency, enabling higher detection rates without additional collecting areas. For example, replacing the baseline configuration ( $N_{\text{st}} = 512$ ,  $D_{\text{st}} = 40 \text{ m}$ ) with ( $N_{\text{st}} = 8192$ ,  $D_{\text{st}} = 10 \text{ m}$ ) substantially increases the number of detectable HzRLQs and raises the detection redshift

limit. However, this improvement comes with greater demands on real-time data transmission, onboard storage, calibration, and computing infrastructure—particularly challenging for a Moon-based observatory.

In summary, the detectability of HzRLQs depends sensitively on array configuration, frequency resolution, and survey design. Continuum surveys provide broad coverage with high signal-to-noise, while 21-cm forest observations offer detailed spectral information at the cost of sensitivity. Both modes benefit from careful optimization of array layout and observing parameters. Future efforts should focus on improving models of high-redshift quasar obscuration, refining array deployment strategies, and developing scalable data processing pipelines. With these advancements, a lunar low-frequency interferometer could open a powerful new observational window into the reionization era, enabling high-precision studies of structure

formation, dark matter, and the thermal history of the early Universe.

### Acknowledgments

This research was supported by multiple funding sources: the National SKA Program of China (2022SKA0110200, 2022SKA0110203), the National Natural Science Foundation of China (12473091, 12473001), and the National 111 Project (B16009). YL acknowledges the support of the Fundamental Research Funds for the Central Universities (No. N2405008). We express our gratitude to ChatGPT for its assistance in refining the manuscript and enhancing the code to improve execution efficiency.

- 
- [1] J. R. Pritchard and A. Loeb, *Physical Review D* **78**, 103511 (2008), 0802.2102.
- [2] Y. Shao, Y. Xu, Y. Wang, W. Yang, R. Li, X. Zhang, and X. Chen, *Nature Astronomy* **7**, 1116 (2023), 2307.04130.
- [3] L. Lopez-Honorez, O. Mena, Á. Moliné, S. Palomares-Ruiz, and A. C. Vincent, *Journal of Cosmology and Astroparticle Physics* **2016**, 004 (2016), 1603.06795.
- [4] S. R. Furlanetto, S. Peng Oh, and F. H. Briggs, *Physics Reports* **433**, 181–301 (2006), ISSN 0370-1573, URL <http://dx.doi.org/10.1016/j.physrep.2006.08.002>.
- [5] J. R. Pritchard and A. Loeb, *Reports on Progress in Physics* **75**, 086901 (2012), ISSN 1361-6633, URL <http://dx.doi.org/10.1088/0034-4885/75/8/086901>.
- [6] T.-Y. Sun, Y. Shao, Y. Li, Y. Xu, and X. Zhang, arXiv e-prints arXiv:2407.14298 (2024), 2407.14298.
- [7] Y. Shao, T.-Y. Sun, M.-L. Zhao, and X. Zhang, arXiv e-prints arXiv:2411.17094 (2024), 2411.17094.
- [8] X.-B. Wu, F. Wang, X. Fan, W. Yi, W. Zuo, F. Bian, L. Jiang, I. D. McGreer, R. Wang, J. Yang, et al., *Nature* **518**, 512–515 (2015), ISSN 1476-4687, URL <http://dx.doi.org/10.1038/nature14241>.
- [9] X. Ding, M. Onoue, J. D. Silverman, Y. Matsuoka, T. Izumi, M. A. Strauss, K. Jahnke, C. L. Phillips, J. Li, M. Volonteri, et al., *Nature* **621**, 51–55 (2023), ISSN 1476-4687, URL <http://dx.doi.org/10.1038/s41586-023-06345-5>.
- [10] Q. Niu, Y. Li, Y. Xu, H. Guo, and X. Zhang, *The Astrophysical Journal* **978**, 145 (2025), ISSN 1538-4357, URL <http://dx.doi.org/10.3847/1538-4357/ad9b97>.
- [11] J. Lazio, C. Carilli, J. Hewitt, S. Furlanetto, and J. Burns, in *UV/Optical/IR Space Telescopes: Innovative Technologies and Concepts IV*, edited by H. A. MacEwen and J. B. Breckinridge (2009), vol. 7436 of *Society of Photo-Optical Instrumentation Engineers (SPIE) Conference Series*, p. 74360I.
- [12] C. W. James, R. D. Ekers, J. Álvarez-Muñiz, J. D. Bray, R. A. McFadden, C. J. Phillips, R. J. Protheroe, and P. Roberts, *Physical Review D* **81**, 042003 (2010), 0911.3009.
- [13] J. Hibbard, in *American Astronomical Society Meeting Abstracts* (2025), vol. 245 of *American Astronomical Society Meeting Abstracts*, p. 344.01D.
- [14] M. Klein Wolt, A. Aminaev, P. Zarka, J.-R. Schrader, A.-J. Boonstra, and H. Falcke, *Planetary and Space Science* **74**, 167–178 (2012), ISSN 0032-0633, URL <http://dx.doi.org/10.1016/j.pss.2012.09.004>.
- [15] J. Burns, G. Hallinan, T.-C. Chang, M. Anderson, J. Bowman, R. Bradley, S. Furlanetto, A. Hegedus, J. Kasper, J. Kocz, et al., arXiv e-prints arXiv:2103.08623 (2021), 2103.08623.
- [16] R. S. Polidan, J. O. Burns, A. Ignatiev, A. Hegedus, J. Pober, N. Mahesh, T.-C. Chang, G. Hallinan, Y. Ning, and J. Bowman, *Advances in Space Research* **74**, 528 (2024), 2404.03840.
- [17] T. B. H. Kuiper, D. L. Jones, M. J. Mahoney, and R. A. Preston, in *Astrophysics from the Moon*, edited by M. J. Mumma and H. J. Smith (AIP, 1990), vol. 207 of *American Institute of Physics Conference Series*, pp. 522–527.
- [18] X. Chen, F. Gao, F. Wu, Y. Zhang, T. Wang, W. Liu, D. Zou, F. Deng, Y. Gong, K. He, et al., *Philosophical Transactions of the Royal Society of London Series A* **382**, 20230094 (2024), 2403.16409.
- [19] S. Iguchi, T. Yamada, Y. Yamasaki, T. Onishi, D. Yamauchi, F. Tsuchiya, K. Takahashi, T. Matsumoto, N. Isobe, T. Iwata, et al., in *Space Telescopes and Instrumentation 2024: Optical, Infrared, and Millimeter Wave*, edited by L. E. Coyle, S. Matsuura, and M. D. Perrin (2024), vol. 13092 of *Society of Photo-Optical Instrumentation Engineers (SPIE) Conference Series*, p. 130922L.
- [20] R. K. Sheth and G. Tormen, *Monthly Notices of the Royal Astronomical Society* **329**, 61 (2002), astro-ph/0105113.
- [21] S. Wyithe and A. Loeb, *The Astrophysical Journal* **595**, 614 (2003), URL <https://api.semanticscholar.org/CorpusID:14629589>.
- [22] Y. Matsuoka, M. A. Strauss, N. Kashikawa, M. Onoue, K. Iwasawa, J.-J. Tang, C.-H. Lee, M. Imanishi, T. Nagao, M. Akiyama, et al., *The Astrophysical Journal* **869**, 150 (2018), 1811.01963.
- [23] Y. Matsuoka, M. Onoue, K. Iwasawa, M. A. Strauss, N. Kashikawa, T. Izumi, T. Nagao, M. Imanishi, M. Akiyama, J. D. Silverman, et al., *Astrophysical Journal Letters* **949**, L42 (2023), 2305.11225.
- [24] D. Stern, S. G. Djorgovski, R. A. Perley, R. R. de Carvalho, and J. V. Wall, *The Astronomical Journal* **119**, 1526 (2000), astro-ph/0001394.
- [25] E. Bañados, B. P. Venemans, E. Morganson, J. Hodge, R. Decarli, F. Walter, D. Stern, E. Schlafly, E. P. Farina, J. Greiner, et al., *The Astrophysical Journal* **804**, 118 (2015), 1503.04214.
- [26] Y. Liu, R. Wang, E. Momjian, E. Bañados, G. Zeimann, C. J. Willott, Y. Matsuoka, A. Omont, Y. Shao, Q. Li, et al., *The*

- Astrophysical Journal **908**, 124 (2021), 2012.07301.
- [27] L. Fanciullo, V. Guillet, F. Boulanger, and A. P. Jones, *Astronomy & Astrophysics* **602**, A7 (2017), ISSN 1432-0746, URL <http://dx.doi.org/10.1051/0004-6361/201630373>.
- [28] H.-L. Guo, B.-Q. Chen, H.-B. Yuan, Y. Huang, D.-Z. Liu, Y. Yang, X.-Y. Li, W.-X. Sun, and X.-W. Liu, *The Astrophysical Journal* **906**, 47 (2021), ISSN 1538-4357, URL <http://dx.doi.org/10.3847/1538-4357/abc68a>.
- [29] W. Li, K. Inayoshi, M. Onoue, and D. Toyouchi, *The Astrophysical Journal* **950**, 85 (2023), ISSN 1538-4357, URL <http://dx.doi.org/10.3847/1538-4357/acbbbe>.
- [30] Y. Ueda, K. Hiroi, N. Isobe, M. Hayashida, S. Eguchi, M. Sugizaki, N. Kawai, H. Tsunemi, T. Mihara, M. Matsuoka, et al., *Publications of the Astronomical Society of Japan* **63**, S937 (2011), 1109.0852.
- [31] Y. Ueda, M. Akiyama, G. Hasinger, T. Miyaji, and M. G. Watson, *The Astrophysical Journal* **786**, 104 (2014), 1402.1836.
- [32] F. Duras, A. Bongiorno, F. Ricci, E. Piconcelli, F. Shankar, E. Lusso, S. Bianchi, F. Fiore, R. Maiolino, A. Marconi, et al., *Astronomy & Astrophysics* **636**, A73 (2020), ISSN 1432-0746, URL <http://dx.doi.org/10.1051/0004-6361/201936817>.
- [33] Square Kilometer Array Cosmology Science Working Group, D. J. Bacon, R. A. Battye, P. Bull, S. Camera, P. G. Ferreira, I. Harrison, D. Parkinson, A. Pourtsidou, M. G. Santos, et al., *Publications Astronomical Society of Australia* **37**, e007 (2020), 1811.02743.
- [34] M. Tarenghi, *Astrophysics and Space Science* **313**, 1–7 (2007), ISSN 1572-946X, URL <http://dx.doi.org/10.1007/s10509-007-9602-9>.
- [35] B. Wang, X. Zhu, C. Gao, Y. Bai, J. W. Dong, and L. J. Wang, *Scientific Reports* **5**, 13851 (2015), 1504.05633.
- [36] T. An, *Science China Physics, Mechanics, and Astronomy* **62**, 989531 (2019), 1901.07756.
- [37] S. Wang, S. Prunet, S. Mignot, and A. Ferrari, *Astronomy & Astrophysics* **692**, A61 (2024), ISSN 1432-0746, URL <http://dx.doi.org/10.1051/0004-6361/202449921>.
- [38] Y. Huang, X.-P. Wu, Q. Zheng, J.-H. Gu, and H. Xu, *Research in Astronomy and Astrophysics* **16**, 016 (2016), ISSN 1674-4527, URL <http://dx.doi.org/10.1088/1674-4527/16/2/036>.
- [39] <https://www.skao.int/en/explore/telescopes/SKA-Low>